NSF Research Experience for Undergraduates (REU) Program
Columbia University Department of Mechanical Engineering
Advanced Manufacturing Laboratory
Veronica Over, Dr. Y. Lawrence Yao

Laser Shock Peening

Justin Donovan

Summer 2021

Table of Contents

Acknowledgements

I would like to thank Dr. Yao and Veronica Over for providing me with a very productive and informative REU program this summer. Although we had anticipated some hurdles, communicating virtually and losing the hands on lab experience, their help and accessibility were always great. Available at any hour, they were never out of reach despite the distance and remote platform. They patiently answered and navigated any questions I had regarding technical difficulties, as well as, software issues, and met with me on very short notice. The Advanced Manufacturing Lab was a perfect place for me to grow as an engineering student, a researcher and a professional. I could not have asked for better mentors, researchers and teachers to learn from and I am extremely grateful for the opportunity to work with them.

Abstract

The objective of this paper is to research, replicate (with a Finite Element Analysis software: Abaqus), and analyze Laser Shock Peening (LSP). LSP is a process that enhances the mechanical properties of a metal sample, and is generally applied after the machining process. One of the most advantageous outcomes of LSP is the compressive residual stress (CRS) that is used to enhance the fatigue life of an object, as well as, hamper crack propagation. This paper will use Abaqus, along with an extensive understanding of the intricacies of LSP, to accurately model LSP and ultimately explore the compressive residual stress imparted on a substrate. This is done to determine the optimal overlap to use in the LSP process. To conclude, we look to the future of LSP, more specifically hybrid manufacturing. We do this to consider the potential for platforms that allows the machining process and the LSP process to work concurrently to achieve a synergistic effect. Through analysis of the anisotropy and grain boundaries, we discuss how the hybrid manufacturing process with LSP, otherwise known as 3D LSP, impacts the material properties.

List of Figures

List of Tables

1 Introduction

Laser shock peening (LSP) is a post processing treatment that is applied to finished surfaces to improve the mechanical properties of a sample. It is a local treatment, meaning that it only affects the region it is applied to, and it is popular to treat fatigued areas, areas of high stress, awkward geometries that might threaten the integrity of the part (fillets and holes), and areas that might undergo wear from continuous impact with debris [1]. In this paper we aim to advance the growth of LSP by exploring both the optimal overlap required between shocks, using a Finite Element Analysis software (Abaqus), and new applications for LSP along with their benefits.

By imparting a compressive residual stress (CRS) on not just the surface, but deeper, LSP works to hamper the propagation of cracks that might originate from small surface defects. As a result, we have great fatigue improvements that have been reported to be as large as 40x the fatigue life of small cracks that do not have the LSP treatment [1]. This relatively new technology is still being researched through altering the apparatus settings, as well as, enhancing laser technology. The settings that vary are the laser intensity, the spot size, the clear overlay material, the opaque overlay material, the material of the substrate, the percent overlap etc [4].

2 Theory

2.1 Mechanical Process

LSP is purely a mechanical process that enhances the material properties of any sample significantly. The components of the apparatus that are necessary to both successfully, and efficiently apply LSP to a surface are as follows: a clear overlay, an opaque overlay (ablative

layer), a laser, and a sample to work on. The laser that is commonly used has a gaussian distribution.

The process begins by directing a pulsed laser beam through the clear overlay, and into the opaque overlay that lays on the top of the surface of the sample. This results in the opaque overlay vaporizing and producing plasma. As the plasma adiabatically expands, it imparts a sudden pressure on the surface of the sample/substrate [1]. This surface pressure results in a shock wave that emanates through the material, and if the stress of the shock wave exceeds a certain threshold, we get plastic deformation.

This limit is better known as the Hugoniot Elastic Limit (HEL), and the plastic deformation only occurs to depths where HEL is less than the stress induced on the material by the shock wave [3]. Another result of LSP that is imparted on the sample is a biaxial compressive residual stress that is on the surface, as well as, deeper along the plane that is parallel to the surface of the object [3]. This biaxial compressive residual stress is advantageous in slowing crack propagation, and results in resistance to wear from foreign objects and an improved fatigue life.

One thing to note is that this process is possible without the clear overlay, however, when it is present it can make the shock wave up to 5x larger, and the pressure last 2-3x longer [2]. This is because the clear overlay does not inhibit the laser, but instead, slows the plasma from escaping into the atmosphere [1]. When determining the yield strength of an object, it is important to take into account the strain rate, because as the strain rate increases, so does the yield strength, making it more challenging for the material to undergo plastic deformation.

2.2 Our Laser

The laser used in the majority of instances of LSP is a high intensity laser $10^8 - 10^9 \; to \; 10^{15} \; W/(cm^2)$ with a Gaussian distribution of intensity, pulses of 15-30 nanoseconds, $1.06 \; \mu m$, and a varying spot size up to 25 mm [1]. Laser intensity can have many distributions, two of which are the "top hat" model, where it is the same throughout the space of the spot, and the gaussian distribution.

Our laser's intensity is a gaussian distribution that varies with space and time. The intensity that we use is 12 $GW/(cm^2)$ because the desired pressure that we wish to impart on the surface of the substrate is 6 GPa. The laser has a spot size with a radius of 0.1 mm, a pulse width of 10 ns, and a repetition rate of 100 Hz.

Below are graphs that demonstrate the pressure profile as it relates to distance from the center of the shock, and time as the laser is turned on and off. In this graph, we used an approximation for the pressure buildup and decay with respect to time. This approximation was a linear buildup and decay and, like the Gaussian distribution of the intensity, we have a peak for the pressure that occurs at the exact halfway time of the laser pulse. We set the maximum intensity to be 12 $GW/(cm^2)$to yield a pressure of $6 * 10^9$ Pa, or 6 GPa in the Abaqus simulation.

```
P0 = 6*10^9;
t1 = (0:1*10^(-3):3.5);
t2 = (3.5:1*10^(-3):7);
p1 = P0*t1/3.5;
p2= P0*(1-(t2-3.5)/3.5);
plot(t1,p1)
xlabel('Time')
ylabel('Pressure (Pa)')
title('Pressure vs Time')
hold on
plot(t2,p2)
```

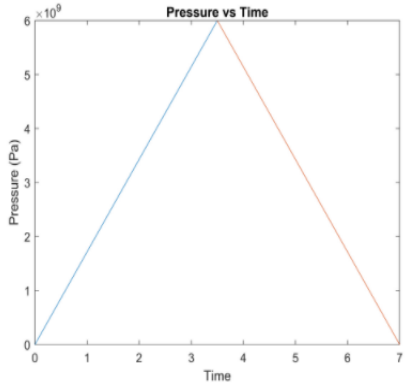

Figure 1: Pressure vs Time

Following this is a graph that demonstrates the pressure profile of the shock as it varies spatially.

```
R0=.1*10^3

R0 = 100

P0 = 6*10^9;
p11 = P0;
p22 = P0/2;
t1 = (0:1*10^(-3):3.5);
t2 = (3.5:1*10^(-3):7);
p1 = P0*t1/3.5;
p2= P0*(1-(t2-3.5)/3.5);
x = (-100:1:100);
F1=p11*(exp(-((x.^2)/2/(R0^2))));
F2=p22*(exp(-((x.^2)/2/(R0^2))));
plot(x,F1)
xlabel('Distance (mm)')
ylabel('Pressure (Pa)')
title('Pressure vs Distance')
hold on
plot(x,F2)
```

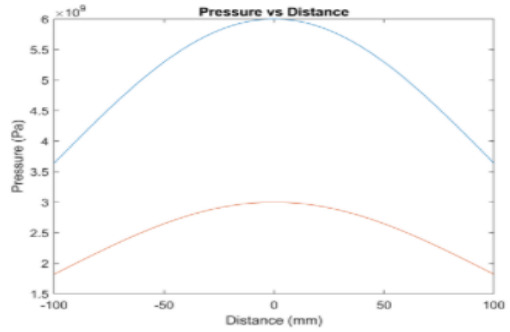

Figure 2: Pressure vs Distance

We note that the two lines are snapshots of how the pressure varies at a given time. We see that the blue line is the pressure as it varies with space when we are at a time with maximum pressure, and the orange line occurs at a time when we have one half of the maximum pressure.

We can see that the orange line has a more gradual curvature while we have a steeper slope on the blue line, demonstrating that as the pressure increases, we have a more drastic change as we leave the center. Thus, when we have a lower pressure, as in the orange line, the pressure does not vary as drastically throughout the affected zone. Therefore, the impact of LSP, as well as how it varies through space, depends on the magnitude of its pressure. When the pressure is larger, we get less of a uniform result in how it behaves on the surface of the substrate.

2.3 Residual Stresses

In the manufacturing process, tensile residual stresses (TRS) are harbored in many manufactured parts. This tensile residual stress is known to be detrimental to the mechanical properties and fatigue life of a manufactured component, and can lead to the formation of cracks [5]. One of the main desires of post processing treatment is to relieve this TRS by imparting what is known as a compressive residual stress (CRS) on the object. This is measurable through a process called x-ray diffraction, where either the surface is analyzed, or a thin layer of the sample

is removed with electropolishing: a very non-intrusive process that imparts no stress on the sample [1]. This process measures the elastic residual strain in materials by using what is known as Bragg's law, and measures the distance between lattice planes. Through the Bragg's angle shift we can tell the elastic strain in the lattice structure [7]. From these strains we can calculate our residual stresses. Therefore, laser shocks cause shockwaves resulting in plastic deformation. This plastic deformation causes residual elastic strain which is ultimately what is seen through the x-ray diffraction. Electron backscatter diffraction measurements (EBSD) is used to observe plastic changes to the microstructure [13].

The CRS is a result of plastic straining and is defined as a biaxial stress along the (001) plane in the S11 and S22 directions [6]. CRS' main function is to deter the propagation of cracks along the surface, however, a deeper CRS is proven to be more effective at increasing the fatigue life of a manufactured part [1]. We note that with a Gaussian loading, the residual stress field is mostly compressive. Therefore, potential cracks at the grain boundary tend to close, proving that LSP may be beneficial for extending fatigue life of components under cyclic loading [13]. Because LSP results in a deeper CRS than its post process counterparts, it is among the most desirable. However, it can be an expensive means of post-process treatment.

3 Apparatus and Approach

3.1 Abaqus Model

Abaqus is a finite element analysis software that uses computer aided design and modeling to analyze various behaviors of the model as it is tested through various user designed loadings. This software is capable of things such as static stress analysis, quasi-static analysis, implicit dynamic analysis, explicit dynamic analysis, uncoupled heat transfer analysis, fully coupled thermal-stress analysis, coupled thermal-electrical analysis, and even computational

fluid dynamics [9]. Here we discuss how we constructed the size, shape, material properties, boundary conditions, loads, steps, and subroutine for the Abaqus to accurately replicate the LSP process. We begin with a 3D deformable model that is both dynamic, and implicit.

3.1.1 Material and Size

For our model, we took a sample that was 1x4x0.15 mm, and assigned it a material with user defined properties that is supposed to have the same mechanical properties as an austenitic (FCC) sample of steel. I began by selecting "part" in the feature tree, and designing a rectangular substrate with the same dimensions as the sample that I intended to replicate. Next, I put in the temperature dependent properties of austenitic steel that has a FCC lattice structure, such as its Young's Modulus, Poisson's Ratio, Yield Stress, Plastic strain, Yield Stress Ratio, and Plastic Strain Rate. I also assigned the material a density that was not temperature dependent. One thing to note is that during the work hardening process, the temperature of the substrate can elevate.

Although the sample is the only part to the assembly, we still need to place it in the assembly for Abaqus to recognize the part in the step. Therefore, I selected "assembly" and then selected the part that I created to populate my sample. Because we want to replicate our real world sample, we define the section to be a solid and homogenous section.

3.1.2 Steps

Next in the cadence of developing an abaqus model, is creating the appropriate steps to allow the substrate to undergo the proper loadings. In each step you are responsible for assigning the boundary conditions, as well as, the load that will be imparted on the substrate. First, this

model has an initial step where the basic default settings are used, followed by the steps for each successive shock. The first shock has the load that we defined for step one set as active, as well as, all of the boundary conditions from step one. The second shock, however, has the load from the first step set as inactive, and the load from the second step defined as active. This way, the subroutine is reset for the second shock and can begin in the new location that is defined for the second shock.

3.1.3 Mesh

The mesh is where we create the nodes on the substrate and ultimately what defines the resolution of the object under analysis. With more nodes, the simulation takes much longer, because it needs to calculate the displacement and deformation of each node, however, the output is much more continuous. Along all surfaces parallel to the x-direction, we have 200 equidistant nodes that span the length of the sample as we travel down the sample the long way.

Because we need the most analysis at the center of the shock, we want to have the smallest nodes at this location. Therefore, we chose to place a bias on the planes in the z and y-directions. Doing so, we set the front and top edge (the one the origin is located on) to have the smallest nodes. This allowed us to have adequate accuracy when defining where the shock's center will be. A single bias was used on these edges where we had 10 nodes and a bias ratio of

1:5. The result is the image below.

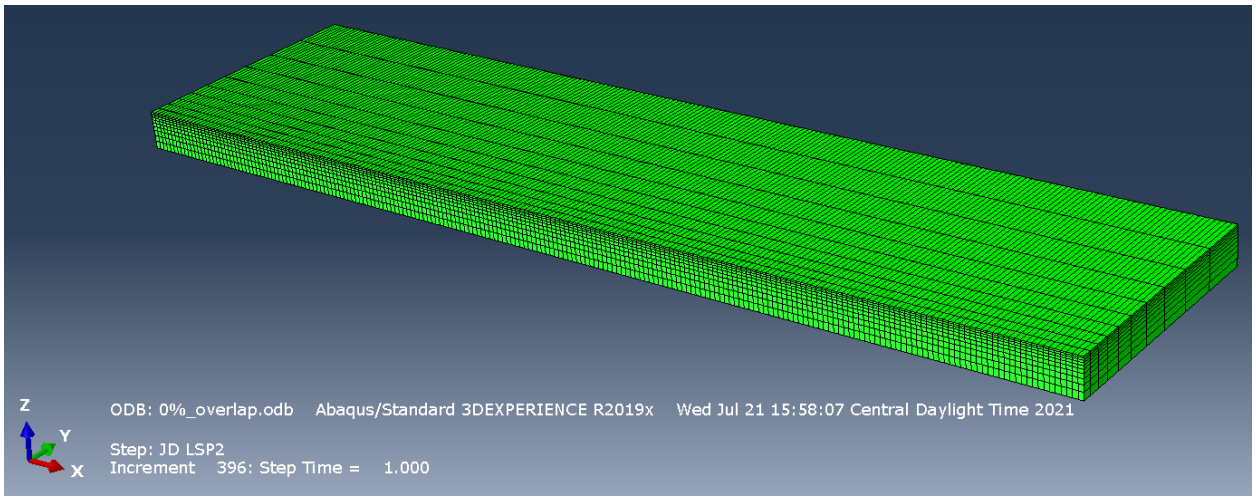

Figure 3: Abaqus Mesh for Substrate

Here we can see that the top/front edge has the smallest nodes and they become progressively larger as we move down the y and z-axis'. We also can see the equidistant spacing as we move across the sample on the x-axis.

3.1.4 Boundary Conditions

Here we employ two different types of boundary conditions. The first that we use is a displacement/rotation boundary condition. We apply this to specific sides of the substrate to replicate how the sample will be fixed in a real LSP experiment. Therefore, the sample has a platform under it and will not move laterally in either direction parallel to the surface. We also fix all rotations. These boundary conditions allow the shock to be fully absorbed by the sample as it would be in a real LSP apparatus.

The second boundary condition that we use is a symmetry boundary condition. This is predominantly used for efficiency and convenience. The symmetry boundary condition is best

when there is a recognizable line of symmetry in the simulation, and in our case, that is along the x-axis. This is because the distance between the different shocks only varies along the x axis, and allows us to only simulate half of each shock, because the other half of it is identical (as seen in the image below).

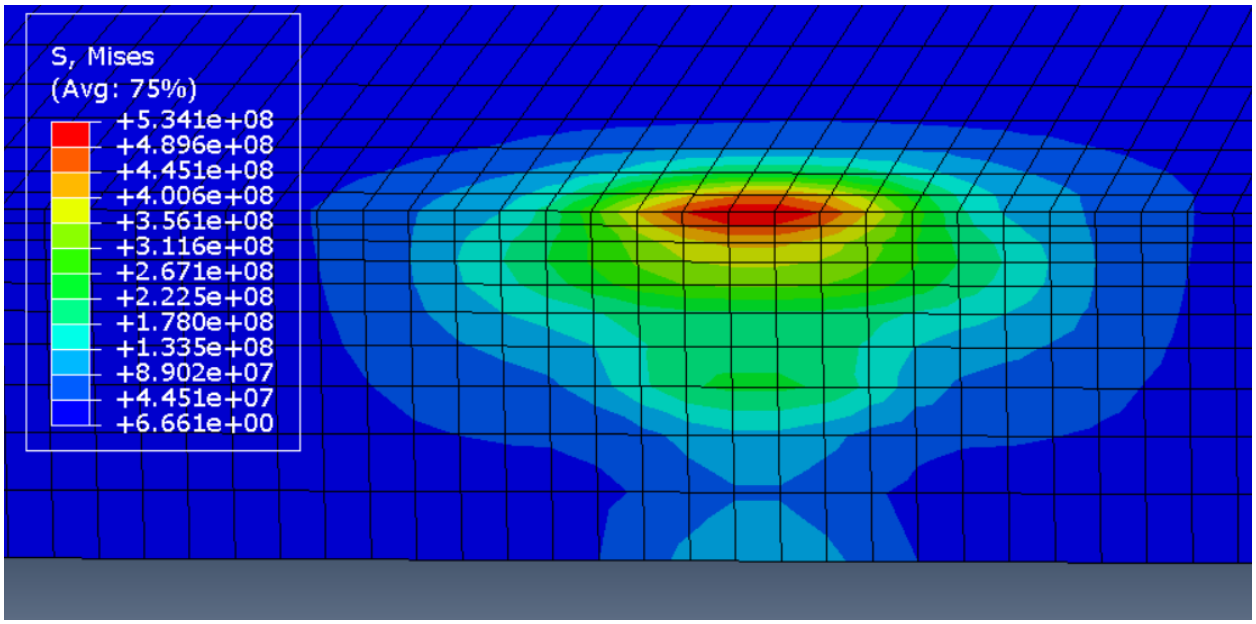

Figure 4: Image of Stress (One Shock)

By only simulating half of the shock, we save a significant amount of time running the simulation.

3.1.5 Load

Knowing the basics of LSP, I chose pressure as the applied load, because the ablative layer becomes plasma and adiabatically expands, providing an immediate pressure on the substrate that forms a shock-wave. The desired peak pressure is 6 GPa, and this is achieved with a laser that has an intensity of 12 $\frac{GW}{cm^2}$.

3.1.6 Subroutine

The subroutine used here is called on in the loading section, more specifically when we select "user defined." This routine is written in FORTRAN, and incorporates the simplified linear buildup and decay of the pressure with respect to time. The subroutine also uses the pressure vs space distribution that we previously defined. It not only applies the pressure that we use for the load to the substrate, but it also specifies the location that this is applied at. The location is dependent on the step, allowing abaqus to move the second shock in the x-direction as desired. This subroutine can be found in the appendix.

3.2 Analysis

In LSP, the most significant components to analyze are the pressure (P(t)), the intensity (I(t)), the plasma thickness (L(t)), the impedance (Z), the constant fraction of internal energy (α), and the internal energy $E_i(t)$. We begin with the equation for the impedance, and define Z_1as the impedance of the metal, and Z_2as the impedance for the clear overlay [2].

$$Z = 2/(1/Z_1 + 1/Z_2) \tag{1}$$

The relationship between the plasma thickness and the shock pressure are derived [3].

$$\frac{dL(t)}{dt} = \frac{2P(t)}{Z} \tag{2}$$

And from this we note that the pressure and the plasma thickness are proportional. We also have the following equation [3],

$$I(t) = P(t)\frac{dL}{dt} + \frac{[E_i(t)L]}{dt} \tag{3}$$

and finally have [3]

$$P(t) = \frac{2\alpha}{3} E_i(t) \tag{4}$$

And from these we can derive an ordinary differential equation that relates the intensity with the thickness of the plasma. The derivation is as follows:

$$I(t) = P(t)\frac{dL}{dt} + \frac{[E_i(t)L]}{dt}$$

$$P(t) = \frac{2\alpha}{3} E_i(t)$$

$$I(t) = P(t)\frac{dL}{dt} + \frac{3}{2\alpha}\frac{d}{dt}[P(t)L(t)]$$

using the chain rule, we know that

$$\frac{d}{dt}[P(t)L(t)] = P'(t)L(t) + P(t)L'(t)$$

thus plugging that in we get

$$I(t) = P(t)L'(t) + \frac{3}{2\alpha}(P'(t)L(t) + P(t)L'(t))$$

and we know someone

$$L'(t) = \frac{2}{Z}P(t)$$

$$P(t) = \frac{L'(t)Z}{2}$$

therefore,

$$I(t) = \frac{L'(t)Z}{2}L'(t) + \frac{3}{2\alpha}(\frac{ZL''(t)}{2}L(t) + \frac{ZL'(t)}{2}L'(t))$$

$$I(t) = \frac{Z}{2}L'(t)^2 + \frac{3}{2\alpha}(\frac{Z}{2}L''(t)L(t) + \frac{Z}{2}L'(t)^2)$$

$$I(t) = \frac{Z}{2}(L'(t)^2) + \frac{3Z}{4\alpha}(L''(t)L(t)) + \frac{3Z}{4\alpha}(L'(t)^2)$$

Thus

$$I(t) = (\frac{Z}{2} + \frac{3Z}{4\alpha})(L'(t))^2 + \frac{3Z}{4\alpha}L''(t)L(t)$$

or

$$I(t) = (\frac{Z}{2} + \frac{3Z}{4\alpha})(\frac{dL(t)}{dt})^2 + \frac{3Z}{4\alpha}(\frac{d^2L(t)}{dt^2})L(t) \tag{5}$$

Finally, we have an equation where we are able to find the HEL with the dynamic yield strength of a material (σ_y^{dyn}), and the Poisson's ratio (ν) [5].

$$HEL = \left[\frac{1-\nu}{1-2\nu}\right](\sigma_y^{dyn}) \quad (6)$$

As previously defined, the HEL is the point at which the substrate undergoes plastic deformation.

4 Results

4.1 Analysis of One Shock

Below is a curve that shows the stress induced on the sample with respect to time with one shock peen. From this, it is evident that as the shock wave travels through the sample, when it reaches the other side of the sample, it rebounds and the shock wave travels up and back through the sample.

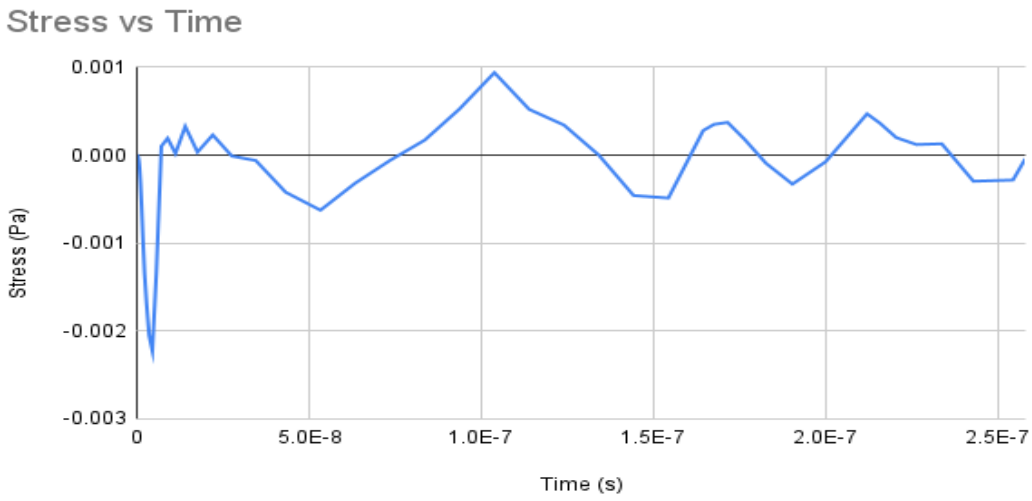

Figure 5: Stress vs Time (One Shock)

Next, we have a graph that demonstrates the behavior of the strain vs time at the center of the shock. We note that the behavior of this is very similar to that of the stress curve, and that is because the stress induced by the shock is what causes this strain. Unlike the stress, the strain graph appears much smoother.

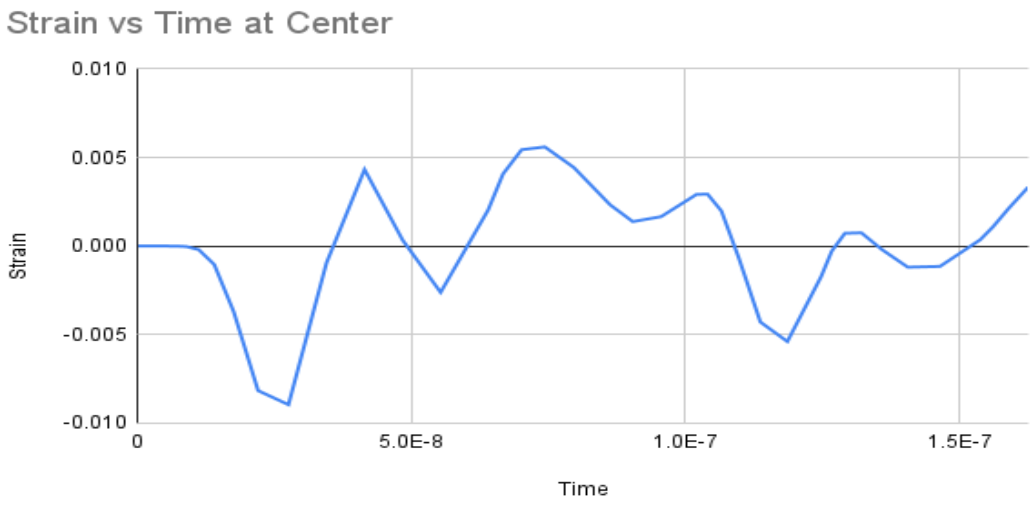

Figure 6: Strain vs Time at Center (One Shock)

Now, when we overlay the two graphs over each other, we can see that the behavior of the stress and strain with respect to time are extremely similar. The strain seems to lag behind the stress and the slope is a little more gradual.

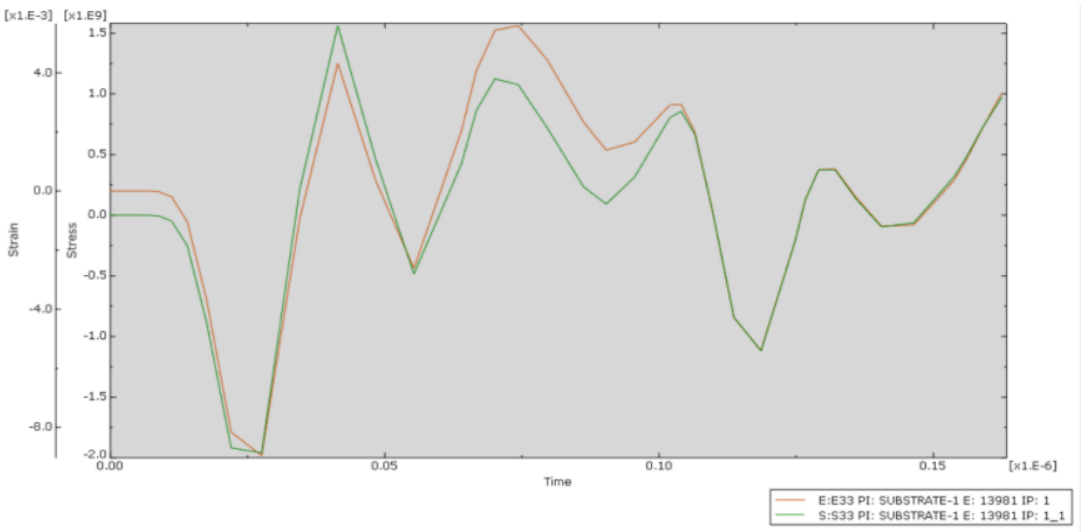

Figure 7: Stress and Strain vs Time (One Shock)

Below, we can see the behavior of the shock waves along the top surface as we step through time. We note that the shock waves oscillate around positive and negative stress, and this is because the thin sample allows the shock waves to rebound and run back through the object. This results in the pattern seen below, where the sample seems to oscillate around zero stress.

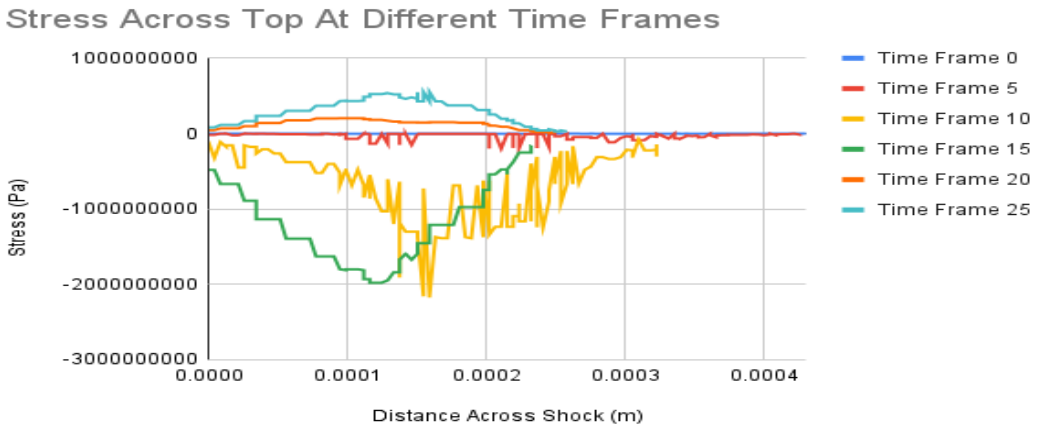

Figure 8: Stress Across Surface At Different Time Frames (One Shock)

4.2 LSP With Overlap

4.2.1 Stress Images

One of our goals of studying LSP with Abaqus is to determine the optimal overlap for LSP on a substrate. To specify, we aim to reduce the tensile residual stress and convert it to compressive residual stress to hamper the crack propagation. Although it seems intuitive that more overlap yields more depth and larger amounts of compressive residual stress, it is also important to use the least time and energy possible. Thus, the goal is to use the least energy while imparting the most compressive residual stress on the substrate. This optimal point is explored through running Abaqus simulations of our LSP model that was explained in detail earlier.

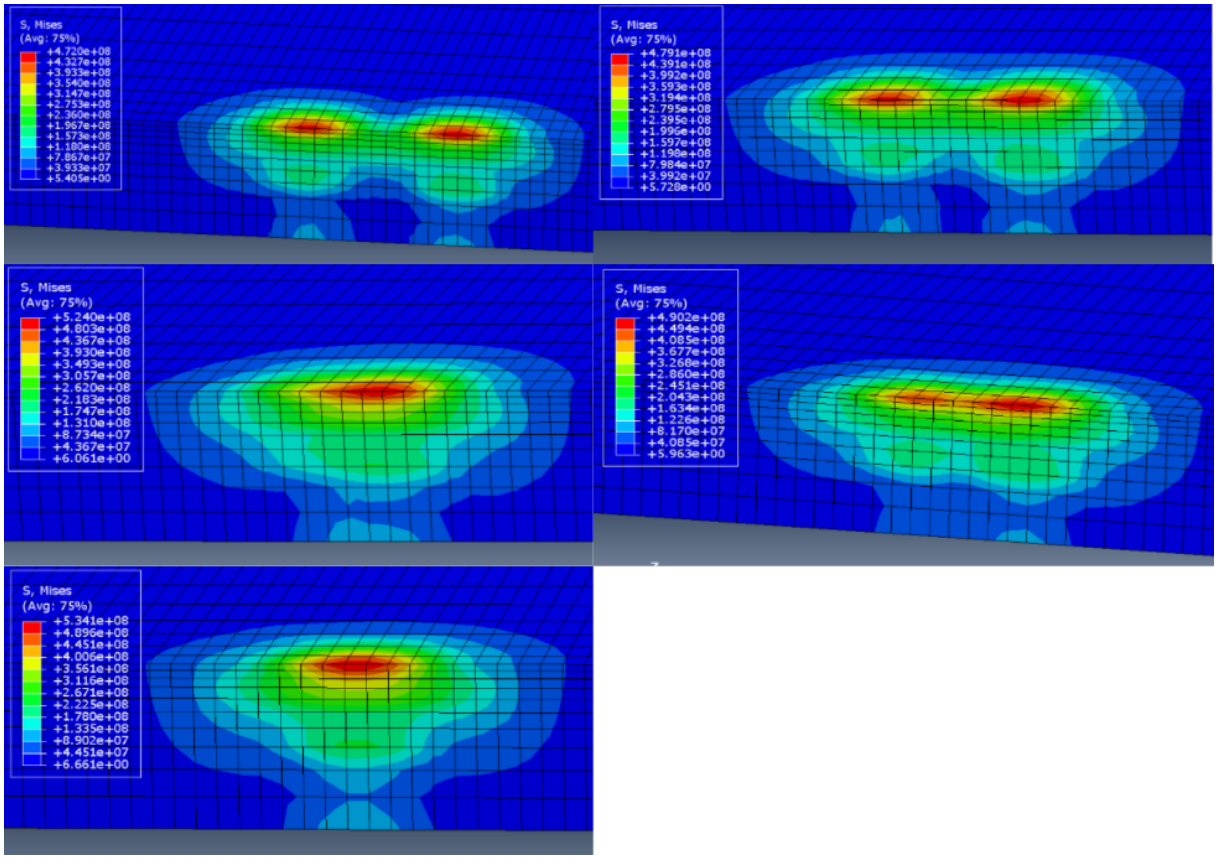

Figure 9: Images of Stresses at Varying Overlaps (Top Left is 0%, Top Right is 25%, Middle Left is 50%, Middle Right is 75%, and Bottom Left is 100%)

Above are images of the stresses on the substrate at varying overlaps. These overlaps represent the percent of the radius that the two spot sizes (both 0.2mm in diameter) overlap.

4.2.2 Stress Varying in the X-Direction

We set the overlap at 0%, 25%, 50%, 75%, and 100% as seen below. The legend corresponds to the depth into the substrate that the stress was found at. In the analysis of this, it is necessary to observe the trade off between the average compressive residual stress on the surface between shocks, the average compressive residual stress at the deepest layer observed between shocks, and finally the maximum and minimum stress experienced by the surface between shocks. These measurements are significant, because they determine the effectiveness of the shock in comparison with how much energy is used in the process. We analyze the surface's weakest compressive residual stress, because, as we know from previously in the paper, fatigue testing is optimized when we can minimize any surface defects, as well as, remove or suppress any abnormalities on the surface. By imparting a CRS on the surface, we are able to reduce the crack propagation significantly and greatly improve the fatigue life of the part.

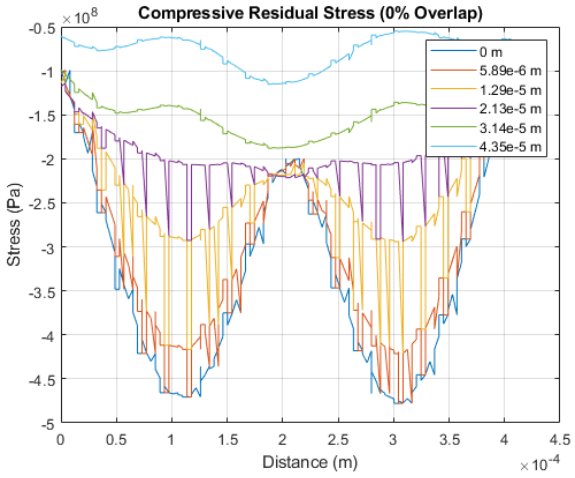

Figure 10: CRS 0% Overlap

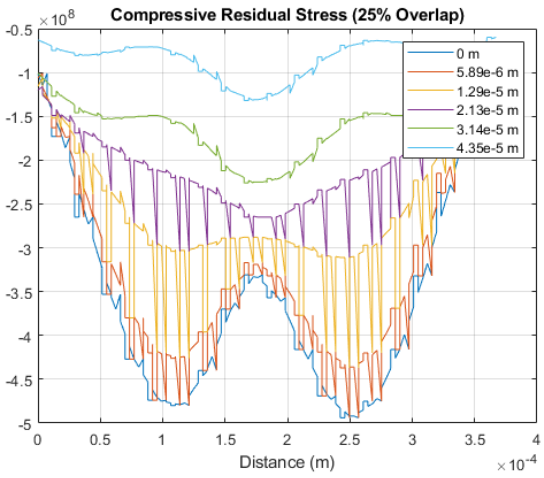

Figure 11: CRS 25% Overlap

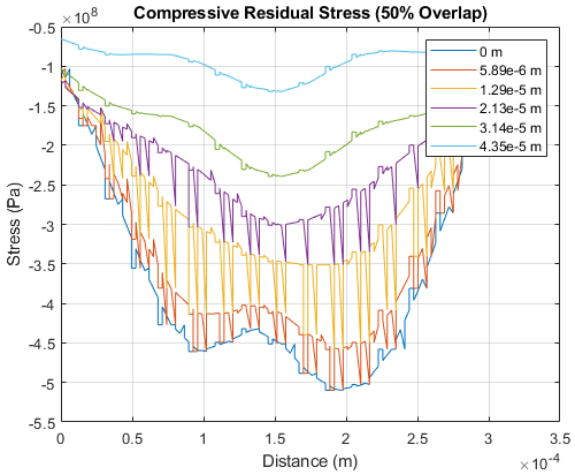

Figure 12: CRS 50% Overlap

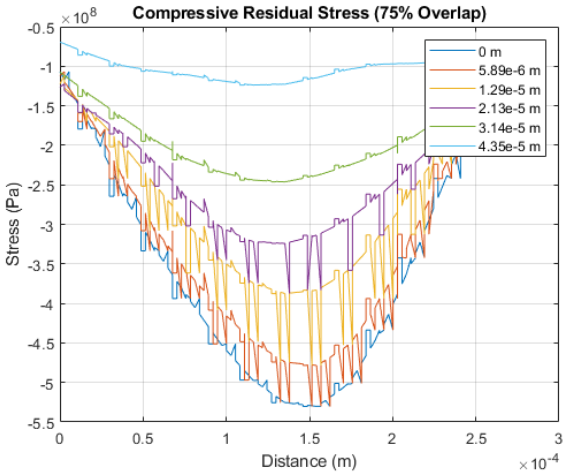

Figure 13: CRS 75% Overlap

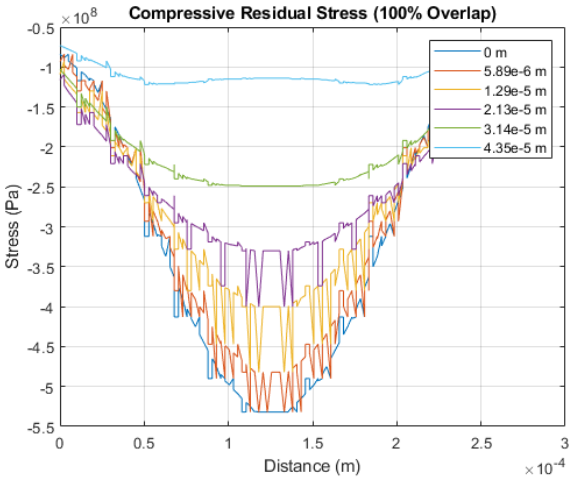

Figure 13: CRS 25% Overlap

From these graphs, we get a better idea of the CRS that is imparted on the sample between shocks. Pulling some of the raw data from this, we decided to look at the compressive residual stress that occurs at both the surface as well as at the 6th node ($4.35 * 10^{-5}\ m$) down. This will give us a better understanding of both CRS on the surface, and CRS deeper into the

sample. The data taken uses the resulting stress in the x-direction or S11 stress so we can see how one of the two biaxial CRS' changes as we vary the percent overlap.

Percent Overlap (Surface)	Average (MPa)	Maximum (MPa)	Minimum (MPa)
0%	353.000	477.881	199.788
25%	411.326	494.135	330.532
50%	463.516	509.826	432.098
75%	510.440	530.238	484.977
100%	319.097	531.751	83.995

Table 1: Overlap Stresses at the Surface

The next table represents the CRS in the 6th node down from the surface or $4.35 * 10^{-5}\ m$ deep into the surface.

Percent Overlap ($4.35 * 10^{-5}\ m$)	Average (MPa)	Maximum (MPa)	Minimum (MPa)
0%	91.643	115.224	54.841
25%	105.653	132.231	68.955
50%	118.189	132.090	99.248
75%	106.976	114.567	101.334
100%	109.561	121.522	72.865

Table 2: Overlap Stresses at the $4.35 * 10^{-5}\ m$ Deep

Finally, the table below demonstrates the energy that the laser uses to achieve the desired pressure, the laser pulse width, the radius spot size, the laser repetition rate and the intensity necessary to achieve the desired pressure. We found that to achieve the desired maximum pressure of 6 GPa, we need an intensity of 12 $\frac{GW}{cm^2}$. Using this intensity, as well as, the area of the spot size we can multiply the two to get our peak power. Now that we have our peak power, we can use the fact that it is a gaussian distribution in conjunction with the laser's repetition rate

(100Hz), the laser's pulse width (10ns), and the radius of the spot (0.1 mm) to find the average power used from the laser. This power is 3.769 W. Then using the percent overlap, we were able to find the number of peens possible on our 4 mm long substrate. Knowing this, as well as the pulse width, we were able to find both the energy usage and time it takes to peen one length of the substrate for the given percent overlaps.

Percent Overlap	Energy Usage (J)	Time (s)
0%	$7.9149 * 10^{-7}$	$2.1 * 10^{-7}$
25%	$1.018 * 10^{-6}$	$2.7 * 10^{-7}$
50%	$1.545 * 10^{-6}$	$4.1 * 10^{-7}$
75%	$3.053 * 10^{-6}$	$8.1 * 10^{-7}$

Table 3: Energy Usage and Time to Shock One Length of the Sample

4.2.3 Stress Varying in the Z-Direction

Here we extracted data from Abaqus that takes the CRS of each shock as it varies in the z-direction in three different places: the center of the first shock, directly between the two shocks, and at the center of the second shock.

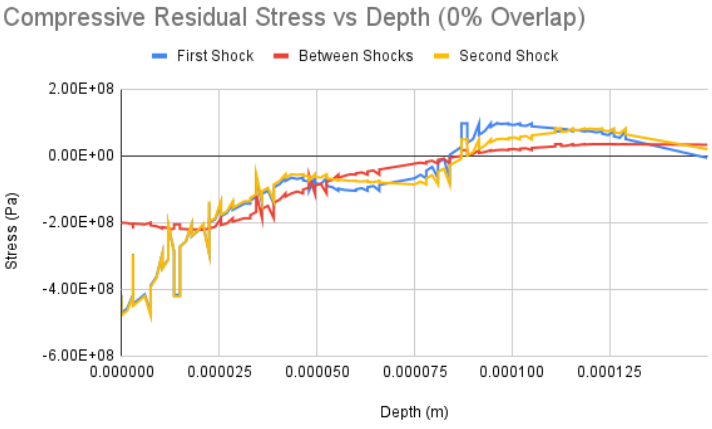

Figure 15: CRS vs Depth, 0% Overlap

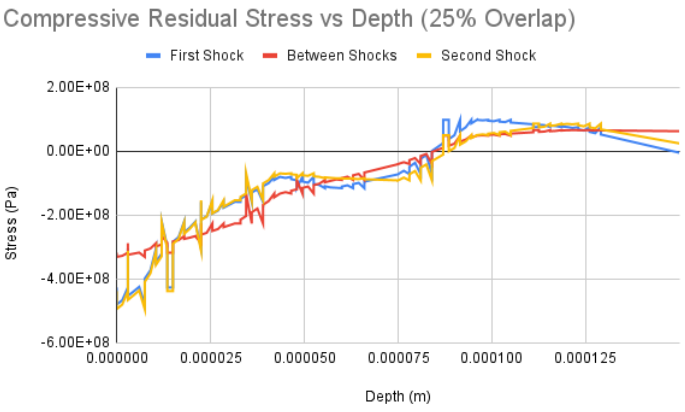

Figure 16: CRS vs Depth, 25% Overlap

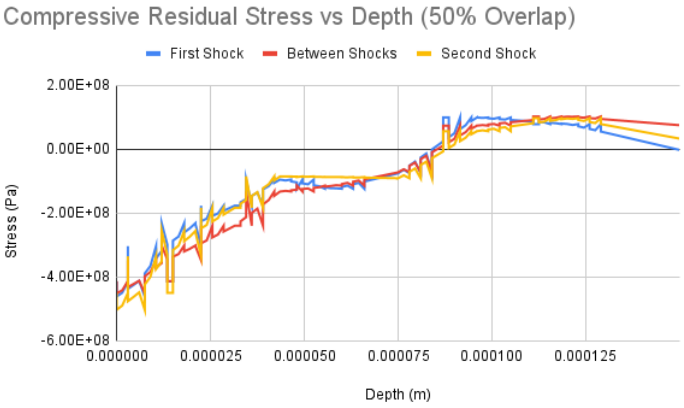

Figure 17: CRS vs Depth, 50% Overlap

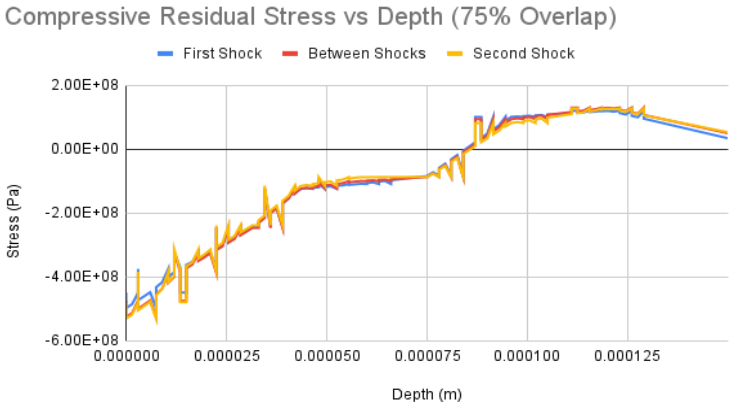

Figure 18: CRS vs Depth, 75% Overlap

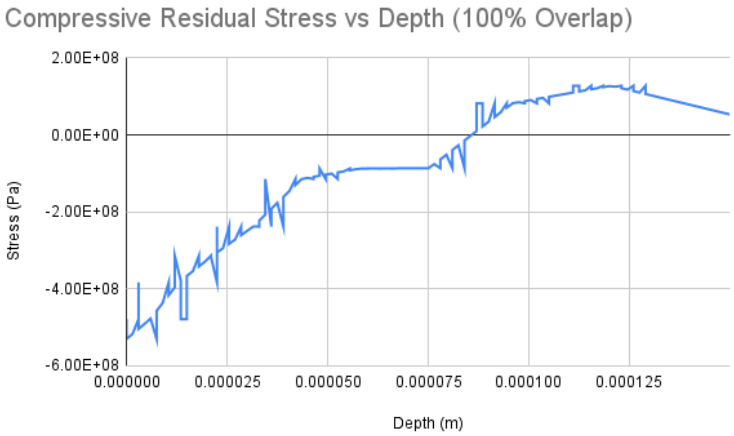

Figure 19: CRS vs Depth, 100% Overlap

5 Discussion of Overlapping Shocks

5.1 Discussion of the Stress Varying in the X-Direction

When trying to determine the optimal overlap, a number of things must be factored in. These range from the maximum, minimum and average CRS at both the surface, and 6 nodes into the sample. We also must account for time spent during the entire LSP process, and the

amount of energy used to treat one length of the sample. It is fair to rule out the 100% overlap immediately, because with it we will not progress along the substrate. Now, looking at the 0% overlap, we notice that along the surface, the minimum CRS is approximately 2.25x less than the maximum. It is known that a relatively uniform CRS is desired on the surface, so it is also fair to state that the 0% overlap model does not have the ideal overlap either. This is because if there is an awkward geometry or wear from debris at the location directly between the shocks, we would have a compromised portion of the sample. Another thing to note is the minimum stress located 6 nodes into the surface for the 0% overlap is 27.4% as strong as at the surface, resulting in a shallow CRS. A shallow CRS can be achieved by other means of treatment, such as shot peening and hot isostatic pressing (HIP). Therefore we can rule the 0% out [11].

Comparing the 75% and the 50% overlap cases, it is noted that the 50% model has 90.8% of the average CRS imparted at the surface that the 75% model does, and only uses 50.6% of the energy. Furthermore, 6 nodes into the sample (or $4.35 * 10^{-5}\ m$ deep) the 50% overlap model actually has a larger average CRS than the 75% model. With a CRS of 118.189 MPa, the 50% model is superior to the 75% model which only has a CRS of 106.976 MPa. Therefore, it is fair to say that the 75% model is less optimal than the 50% model.

Finally, when contrasting the remaining 50% and 25% overlap models, we want to find the percent overlap that retains the most CRS and fatigue life, while also minimizing the time and energy costs. Although the 50% takes a noticeable amount of time and energy (41 shocks to go one length for the 50% model and 27 shocks for the 25% model), we see a much better consistency in the surface CRS. We see the difference between the average CRS and the maximum CRS at the surface to be significantly smaller in the 50% model than we do in the 25% model. Similarly, we also note that the difference between the average CRS and the minimum

CRS is also smaller in the 50% model than it is in the 25% model. The consistency in the surface CRS is what makes the 50% model more desirable than the 25% model. When comparing the 50% model with the 25% model at the deeper depth (6th node) the same consistency appears in the 50% model as it does at the surface. It is also important to add that the 50% model has the largest average CRS at the depth of the 6th node out of all of the models. Therefore, when looking at the CRS as it varies across the shock in the x-direction, it is evident that an overlap of 50% is the most desirable.

5.2 Discussion of the Stress Varying in the Z-Direction

When observing figures 15-19, we observe the behavior of the stress as it begins on the surface of the sample and travels to the bottom. In thicker samples, there is a region in the center of the sample that has a positive compressive residual stress, however, because of the relatively thin thickness of our sample, the positive residual stress occurs at the bottom surface. Positive residual stresses open up surface defects and enhance crack propagation, forcing the cracks to naturally widen. Therefore, it is not desirable to have a positive residual stress on the surface or even close to the surface of any sample. If LSP were to be performed on a sample as thin as ours (.15 mm thick), then peening both sides of the sample will result in a much improved fatigue life. However, when looking at the positive compressive residual stress on the bottom, it dissipates as we remove the overlap, thus demonstrating that if the both sides are not treated, less overlap results in less positive CRS on the bottom surface, making it more desired.

Another observation of figures 15-19 is that when we have less overlap, the between the shocks line tends to deviate from the behavior of the CRS at the first and second shocks. This results in a smaller CRS between the shocks than experienced at the center of the shocks. As the

overlap becomes greater, we can see the behavior of the “between the shocks” line mirror that of the first and second shock lines, resulting in more positive CRS in the bottom, but a more uniform distribution of stress throughout the sample. A relatively uniform residual stress across a treated area is known to be a very important mechanical property [1]

6 The Future of Additive Manufacturing with LSP

6.1 Hybrid Manufacturing

Hybrid manufacturing is defined as cyclically coupling a machining process with a process performance method. The term hybrid machines directly refers to the machine platform itself. On the machine platform we have a system where the process performance method occurs during the machining process and not pre or post machining. Ideally we want the process to be synergistic, more specifically to have a “1+1=3” effect, when the processes happen concurrently [10]. Among the many hybrid manufacturing processes available, we will be focusing on cyclically alternating LSP and 3D printing. This is otherwise known as 3D LSP and is defined as the process when LSP imparts a deep CRS on the machined part in between printed layers.

6.2 3D LSP

The two predominant additive manufacturing processes that use 3D LSP are selective laser manufacturing (SLM) and directed energy deposition (DED) [11]. In SLM, otherwise known as laser powder bed fusion, metal powder is placed on the surface of the part, and melted by a laser to help it adhere to the part. For our other process, DED, we have metal in the form of powder or wire that is melted by a heat source prior to being deposited on a bed or previous layer [10]. Both processes are layered, and this allows LSP to be done between every few layers. One

thing to note is that a downside to SLM is that it results in a tensile residual stress that limits the fatigue life of the part, distorts the geometry of the part, produces cracks and causes delamination. Therefore, with the use of LSP, we are able to relieve some of the detrimental TRS and impart some CRS. This results in the reversal of many of the negative byproducts of SLM. In further research, it was found that the optimal peening for 3D LSP is every 10 layers at 80% overlap [10]. An example to further exemplify the benefits of relieving TRS and imparting CRS in 3D LSP, is that parts that are processed with 3D LSP demonstrate more than 15 times the fatigue life of the samples machined without LSP. This testing was done at a load of 360 MPa [11].

6.3 Additive Manufacturing Anisotropy/Grain Growth

Metal AM Parts have anisotropic and heterogeneous microstructures that are different from the metallic parts manufactured via conventional methods. In metal AM, there are many settings that, if altered, can impact the grain growth, and ultimately change the anisotropic properties of the material. For example, low deposition rates result in better geometry and better resolution of the material deposition, however, higher deposition rates have a greater percentage of equiaxed grains (grains with the same dimensions in all directions) [14]. Another example of this is that varying scan strategies in DED can alter the crystal textures of grains, also leading to potential anisotropic effects in the material. A common microstructure feature observed in metal AM parts was the epitaxial columnar grain morphology. These are parallel to the build direction which ultimately causes anisotropy [14]. This anisotropy stems from a build up of long-range backstress due to slip dislocations piling up in one direction, as well as fewer grain boundaries along one axis and a strong texture. This grain formation is a result of re-melting old layers of

the part as we add on new layers. In horizontally orientated samples, the cracks propagate through the columnar grains, and in vertically orientated samples, cracks propagate along the columnar grain boundary instead. Both of these can be relieved by imparting a CRS via LSP, however, we must look at which way the part is orientated to effectively impart CRS at the proper location [14].

Conclusion

Throughout this paper, we discussed the mechanical process of LSP, the impact it has on the properties of a sample, and the CRS that is transmitted to the sample. Then, applying all of the information gathered, we ran an Abaqus model that accurately replicated the LSP process. With this model, we changed the subroutine to vary the distance between shocks, giving us data on many models with different percent overlaps. With this data, we were able to deduce the optimal CRS based on the average, maximum, and minimum CRS at the surface, as well as, 6 nodes down in the model. We then compared this with the time and energy that each model would take to peen one length of the sample.

We determined that, when analyzing the stress that varies along the x-axis, the model with 50% overlap imparts the most CRS at both the surface, and 6 nodes down, when considering the time and energy spent. We also determined that a sample with less overlap, such as the 25% sample is great for thin substrates such as ours. This is the case, because when we look at how the CRS varies with the z-axis, we see that we have a much larger positive CRS at the bottom of the sample when the overlap is greater. However, this is not the case for thicker substrates, where the shock waves bounce off the bottom surface and travel back to the top. Therefore, for our thin sample if we look across the x-axis, it is evident that the 50% is the ideal

overlap, but if we look at how the CRS varies across the z-axis, we see that the 25% overlap is more desired.

Finally we considered the future of LSP, more specifically with hybrid manufacturing. The hybrid manufacturing process that we focused on is known as 3D LSP, and it is proven to enhance the mechanical properties of machined parts. We note that by machining and imparting LSP simultaneously, we are achieving an even greater desired outcome, than if we were using LSP as a post-process treatment. Hopefully as technology progresses, a hybrid manufacturing platform that joins LSP and machining into one process is both achievable and effective.

Appendix

```
      SUBROUTINE DLOAD(F,KSTEP,KINC,TIME,NOEL,NPT,LAYER,KSPT,COORDS,JLTYP)
      INCLUDE 'ABA_PARAM.INC'
      DIMENSION TIME(2), COORDS(3)
      Real R, R0, P,P0, t,t0, Xc,Yc
C       Xc = 0.0


      If (KSTEP .LT. 2) THEN
C     Determines what step the simulation is on so it can change what location it is in based on step
      Xc = 0.0000e-3
      Yc=0.0000e-3
C     Coordinates of the first shock
C       TIME(1) is the step time.  TIME(2) is the total time. t is step time in nanoseconds
      t=TIME(1)*1.0e9
C     Sets the time in nanoseconds
        t0=7
        R0=0.1*1e-3
C     Sets the radius of the shock to 0.1 mm
        P0=6e9
C     Desired peak pressure
      IF (t .LT. 3.5) THEN
      P=P0*t/3.5
C     Uses a linear build up if our pressure is below the peak pressure
      ELSEIF ((t .GE. 3.5) .AND.  (t .LE. 7)) THEN
C     Uses a linear decay to zero
      P=P0*(1-(t-3.5)/3.5)
      ELSE
        P=0
      ENDIF
      ELSEIF (KSTEP .LT. 3) THEN
      Xc = 0.2000e-3
      Yc = 0.0000e-3
C     Determines what step the simulation is on so it can change what location it is in based on step
C     In the second step we vary this from 0 mm to 0.2 mm depending on the percent overlap desired
C       TIME(1) is the step time.  TIME(2) is the total time. t is step time in nanoseconds
      t=TIME(1)*1.0e9
        t0=7
        R0=0.1*1e-3
        P0=6e9
      IF (t .LT. 3.5) THEN
      P=P0*t/3.5
      ELSEIF ((t .GE. 3.5) .AND.  (t .LE. 7)) THEN
C  use a linear decay to zero
      P=P0*(1-(t-3.5)/3.5)
      ELSE
        P=0
      ENDIF

      ElSE
      P=0
      ENDIF

C  For a line of shocks: 0-400 microns, with 25 micron spacing, along Y idrection

        F=P*( 1*exp( -((COORDS(1)-Xc)**2+(COORDS(2)-Yc)**2 )/2/(R0**2) ) )


      RETURN
      END
```

References

[1] Clauer, Allan, 1997/01/01, "Laser shock peening for fatigue resistance," Conference: Proceedings of a Conference on Surface Performance of Titanium, Volume: Surface Performance of Titanium, pp 217-230

[2] Zhang, Wenwu, and Y. Lawrence Yao. "Micro Scale Laser Shock Processing of Metallic Components." *Journal of Manufacturing Science and Engineering*, vol. 124, no. 2, 2002, pp. 369–378., doi:10.1115/1.1445149.

[3] Fabbro, R., et al. "Physics and Applications of Laser-Shock Processing." *Journal of Laser Applications*, vol. 10, no. 6, 1998, pp. 265–279., doi:10.2351/1.521861.

[4] Fabbro, R., et al. "Physical Study of Laser‐Produced Plasma in Confined Geometry." *Journal of Applied Physics*, vol. 68, no. 2, 1990, pp. 775–784., doi:10.1063/1.346783.

[5] Chattopadhyay, Angshuman, et al. "Effect of Laser Shock Peening on Microstructural, Mechanical and Corrosion Properties of Laser Beam Welded Commercially Pure Titanium." *Optics & Laser Technology*, vol. 133, 2021, p. 106527., doi:10.1016/j.optlastec.2020.106527.

[6] Shukla, Pratik, et al. "Shock-Wave Induced Compressive Stress on Alumina Ceramics by Laser Peening." *Materials & Design*, vol. 167, 2019, p. 107626., doi:10.1016/j.matdes.2019.107626.

[7] Chen, Hongqiang, et al. "Spatially Resolved Characterization of Residual Stress Induced by Micro SCALE Laser Shock Peening." *Journal of Manufacturing Science and Engineering*, vol. 126, no. 2, 2004, pp. 226–236., doi:10.1115/1.1751189.

[8] "Abaqus Tutorials," SIMULEON BY TECHNIA, Available: https://www.simuleon.com/abaqus-tutorials/

[9] "Abaqus/CAE User's Guide," SIMULIA - Dassault Systemes. Available: http://130.149.89.49:2080/v6.14/books/usi/default.htm

[10] Sealy, Michael P., et al. "Hybrid Processes in Additive Manufacturing." *Journal of Manufacturing Science and Engineering*, vol. 140, no. 6, 2018, doi:10.1115/1.4038644

[11] Kalentics, Nikola, et al. "3D Laser Shock Peening – A New Method for Improving Fatigue Properties of Selective Laser Melted Parts." *Additive Manufacturing*, vol. 33, 2020, p. 101112., doi:10.1016/j.addma.2020.101112.

[12] Ebrahimi, Mohammad, et al. "The Investigation of Laser Shock Peening Effects on Corrosion and Hardness Properties of ANSI 316L Stainless Steel." *The International Journal of Advanced Manufacturing Technology*, vol. 88, no. 5-8, 2016, pp. 1557–1565., doi:10.1007/s00170-016-8873-0.

[13] Vukelić, Siniša, et al. “Grain Boundary Response of Aluminum Bicrystal under Micro Scale Laser Shock Peening.” *International Journal of Solids and Structures*, vol. 46, no. 18-19, 2009, pp. 3323–3335., doi:10.1016/j.ijsolstr.2009.04.021.

[14] Kok, Y., et al. “Anisotropy and Heterogeneity of Microstructure and Mechanical Properties in Metal Additive Manufacturing: A Critical Review.” *Materials & Design*, vol. 139, 2018, pp. 565–586., doi:10.1016/j.matdes.2017.11.021.

[15] Nakano, Takayoshi, et al. “Control of Crystallographic Orientation by Metal Additive Manufacturing Process of β-Type Ti Alloys Based on the Bone Tissue Anisotropy.” *MATEC Web of Conferences*, vol. 321, 2020, p. 05002., doi:10.1051/matecconf/202032105002.